AIP | Review of Scientific Instruments

Imaging ferromagnetic tracers with an ac biosusceptometer

M. Moreira, L. O. Murta Jr., and O. Baffa

Citation: Review of Scientific Instruments **71**, 2532 (2000); doi: 10.1063/1.1150666

View online: http://dx.doi.org/10.1063/1.1150666

View Table of Contents: http://scitation.aip.org/content/aip/journal/rsi/71/6?ver=pdfcov

Published by the AIP Publishing

Imaging ferromagnetic tracers with an ac biosusceptometer

M. Moreira,[a] L. O. Murta, Jr., and O. Baffa[b]
Department of Physics and Mathematics-FFCLRP-USP, 14040-901 Ribeirão Preto, SP, Brazil

(Received 27 July 1999; accepted for publication 18 February 2000)

The aim of this work was to study the feasibility of obtaining images of the distribution of ferromagnetic tracers using an ac biosusceptometer (ACB). The images were generated by mapping the response of the ACB at short distances due to the presence of a ferrite powder dispersed in a planar gel matrix with different shapes. The ACB was scanned over the sample and the voltages generated by the variation in ferrite concentration were sampled. Methods to render and image the distribution of ferromagnetic particles were studied. The generalized Wiener parametric method gave the best results. The system has a potential to be used in functional images of the gastrointestinal tract where a moderate resolution is required. We conclude that this biomagnetic method can be successfully used to generate planar functional images of magnetic particles in the near field. © *2000 American Institute of Physics.* [S0034-6748(00)02406-0]

I. INTRODUCTION

Imaging techniques have been very useful in visualizing various phenomena in science and technology. Medical sciences have been benefited in many aspects from images of tissues and organs obtained from a microscopic to a macroscopic scale. Electron and optical microscopy and, more recently, atomic force microscopy and its variants have been used to image tissue preparations and even large molecules, on a micron and submicron scale. X rays, scintilography, ultrasound, and magnetic resonance have been successfully employed to produce anatomical and functional images of organs and are routinely used in hospitals. Other techniques such as: electrical impedance,[1] electron spin resonance,[2,3] and biomagnetic measurements[4,5] are in an experimental stage to produce images of different physical properties and may find in the future a place in the medical environment. In this article we show how images of the distribution of ferromagnetic particles can be obtained by sampling the magnetic susceptibility in a plane. This susceptometric method is based on the use of a magnetic test meal and has been employed in gastroenterology for measurements of gastric emptying,[6] small bowel transit,[7,8] gastric antral contractions,[9] and esophageal transit time.[10] Biomagnetic methods, such as the susceptometric approach employed in this work, have the advantage of the absence of ionizing radiation and of being noninvasive.[11,12] A potential disadvantage is the strong dependence of signal with the distance from the source, leading to a degradation of the signal to noise (S/N) ratio. This image technique could also be used in other areas such as nondestructive evaluation[13] and agriculture[14] to study problems where magnetic tracers can be employed.

In this work, the ac biosusceptometer (ACB) was attached to a scanning device and data were collected on flat phantoms containing a magnetic test meal. Digital images were acquired and the parameters that control the response of the ACB as well as the imaging processing techniques were optimized.

Thus, the main thrust of this work is to present a pilot study of a new imaging method based on the response of an ac biosusceptometer due to the presence of a ferromagnetic tracer at short distances.

II. METHODS

A. The imaging restoration process

The general problem of imaging production can be stated as shown in Fig. 1. An arbitrary object in the image plane can be represented by the function f, and an imaging device characterized by the impulse response h will produce an image g in the image plane. This imaging process does not have a point response, a so-called ideal response; so there is always some distortion present. In many cases the distortion can be visualized as a blurring of the original image. The imaging process can be described in the frequency domain as the convolution between the functions f and h. To restore the original image a deconvolution process will have to be performed. Starting from the object and obtaining the image is usually referred to as the direct problem. In terms of magnetism the direct problem is to calculate the magnetic field generated by a known distribution of properly excited ferromagnetic particles. We are concerned with the opposite, i.e., how to find the distribution of the ferromagnetic particles from the magnetic fields measured in a certain plane, the so-called inverse problem. This process will involve the inversion of function h. The function h may be zero at some points complicating the inversion procedure, because poles may arise. Several methods, such as least squares fitting, minimum norm, minimum entropy and Fourier analysis, have been employed to deal with this problem. Among others we tried the inverse and pseudo inverse filtering, Wiener and generalized parametric Wiener filtering. The last procedure gave the best results in the present work. The standard

[a]Present address: Electrical Engineering Department, UNICAMP, 13083-970 Campinas, SP, Brazil.
[b]Author to whom correspondence should be addressed; electronic mail: baffa@dfm.ffclrp.usp.br

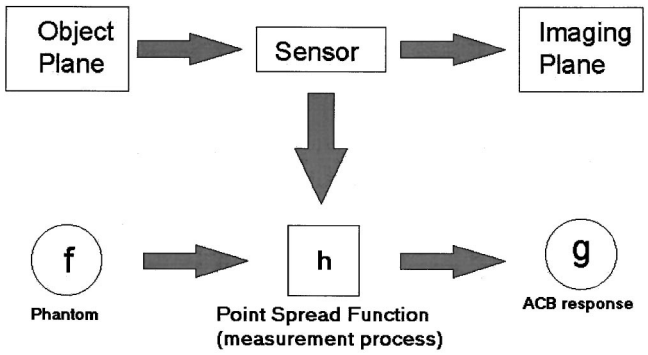

FIG. 1. Schematic diagram summarizing the mathematical concepts of imaging formation, where f is the function representing the object, h the transfer function, h^{-1} its inverse, and g the image. The image can be obtained by convoluting $g=f*h$ and the object restored by convoluting the inverse of the transfer function $f=g*h^{-1}$.

Wiener filter involves the minimization of the root mean square (rms) error between the original and the retrieved image. However, the rms error is not the only criterion that can be used by the observer to judge the quality of the restored image, and many variations have been proposed. In the present work a more general expression for the Wiener filter was employed as follows:[15]

$$W[k_x,k_y]=\left(\frac{|H[k_x,k_y]|^2}{|H[k_x,k_y]|^2+\alpha 10^{-S[k_x,k_y]/10}}\right)^{\beta}\cdot H_{\gamma}^{-1}[k_x,k_y], \tag{1}$$

where α and β are real parameters ($\alpha,\beta>1$), $H_{\gamma}^{-1}[k_x,k_y]$ is the pseudo inverse filter, and $S[k_x,k_y]=10\cdot\log_{10}(P_f[k_x,k_y]/P_{\eta}[k_x,k_y])$ is an expectation of the S/N, where P_f is the power spectrum of the object and P_{η} is the power spectrum of the ambient noise. It is important to note that the parameter α controls the level of the additive noise present in the image as a function of k_x and k_y, the x and y components of the spatial frequency. As this parameter is increased the attenuation of the noise is obtained more effectively. Considering that the filter response is such that $|W[k_x,k_y]|\leqslant 1$, the exponent β allows the selection of the steepness of the filter function. The introduction of the pseudo inverse filter controls the influence of the poles in the deconvolution process by changing the parameter γ that determines the threshold value for $H_{\gamma}^{-1}[k_x,k_y]$.

B. The magnetic field detected by the ACB from point and extended sources

Experimentally the problem of obtaining susceptometric images of a magnetic material distribution involves its magnetization and the measurement of the response to this magnetic field. When one is concerned with a volume, the problem is complicated by the need to selectively excite different *voxels*.[16] This can be accomplished by using magnetic field gradients, localized magnetic fields, and a uniform field applied to a thin sample. Tan *et al.*[17] used a uniform field produced by a solenoid to magnetize the sample and the magnetization was sampled with a superconducting quantum interference device (SQUID) detector. In our case the ACB produces a localized magnetization that spreads a few centimeters deep and wide in the sample, so the present method can be classified as the one that employs localized magnetization. The ac biosusceptometer is shown in Fig. 2, a pair of detecting coils (1,4) or sensors, is coupled to a pair of exciting coils (2,3), in opposite polarity (first order gradiometer) so as to cancel the detected voltage if no ferromagnetic material is nearby.[6] The net voltage detected is amplified by a lock-in amplifier.

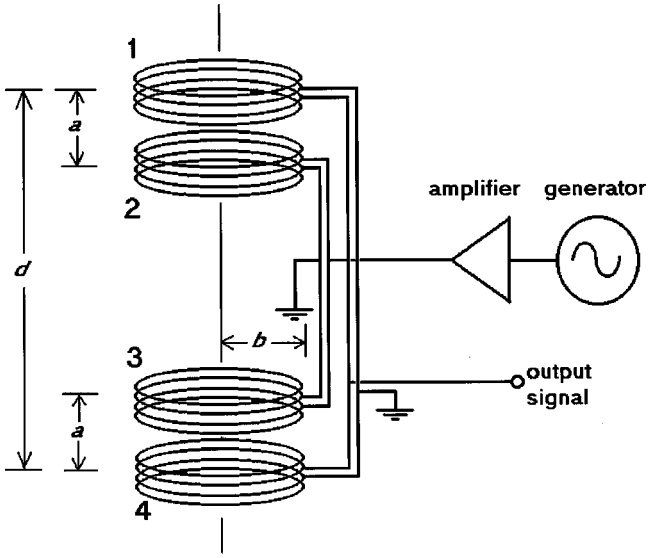

FIG. 2. Schematic diagram of the ac biosusceptometer. The figure shows the detecting (1,4) and exciting (2,3) coils; both have a diameter of 10 mm. The ac biosusceptometer is assembled as a first order gradiometer to cancel the detected voltage if no ferromagnetic material is nearby.

Figure 3 shows a volume element dV located at a distance r from the lower set of coils. This sample can be described as a magnetic dipole of intensity dm_z. To describe this magnetic moment, an auxiliary coordinate system $\hat{x}_1$, $\hat{y}_1$

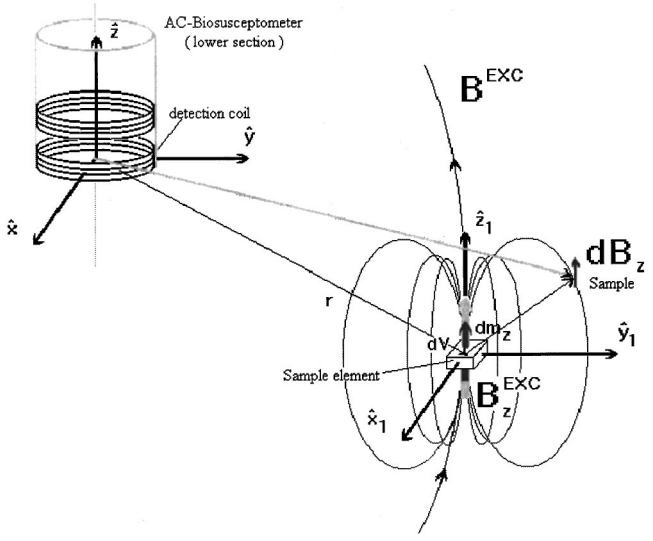

FIG. 3. Coordinate system attached to the lower set of coils and the contribution of an element of volume dV containing the ferromagnetic material, giving a magnetic dipole of intensity dm_z. The (x,y) displacement is exaggerated in this figure, in practice only the z component of the magnetic field is relevant.

and $\hat{z}_1$, centered in the sample will be used to describe the volume of magnetic material by the vector $r'(x',y',z')$. The magnetic field B_z produced by this volume in the ACB is given by[18]

$$dB_z=\frac{\mu_0}{4\pi}\frac{2(z-z')^2-[(x-x')^2+(y-y')^2]}{[(x-x')^2+(y-y')^2+(z-z')^2]^{5/2}}dm_z. \quad (2)$$

Because the sample must be near the detector we assume that only the Z component of the magnetic field will be relevant to determine the response of the ACB due to the presence of the ferromagnetic material. Thus, the magnetic moment can be determined according to

$$dm_z(x',y',z')=M(x',y',z')\cdot dV=\chi(x',y',z')\cdot B_z^{\mathrm{EXC}}(x',y',z',t)\cdot dV, \quad (3)$$

where the term $B_z^{\mathrm{EXC}}(x',y',z',t)$ is the Z component of the magnetic field produced by the action of the two exciting coils in the sample, and is given by

$$B_z^{\mathrm{EXC}}(x',y',z',t)=\frac{\mu_0 I(t)}{4\pi}\pi b^2 N_{\mathrm{EXC}}\left\{\frac{2(z'+a)^2-(x'^2+y'^2)}{[x'^2+y'^2+(z'+a)^2]^{5/2}}+\frac{2[z'+a+(d-2a)]^2-(x'^2+y'^2)}{[x'^2+y'^2+[z'+a+(d-2a)]^2]^{5/2}}\right\}, \quad (4)$$

where $I(t)=I_0\sin(2\pi ft)$ is the alternating current of frequency f applied to the exciting coils with radius b and N_{EXC} turns. The magnetic susceptibility $\chi(x',y',z')$ due to the distribution of ferromagnetic material in this sample is calculated by the following expression:

$$\chi(x',y',z')=\frac{C(x',y',z')}{\rho}\left(\frac{\mu}{\mu_0}-1\right), \quad (5)$$

where ρ is the density, $C(x',y',z')$ is the concentration, μ the magnetic permeability of the ferromagnetic material and μ_0 the vacuum permeability. For thin samples $dV\cong\epsilon dx'dy'$, where ϵ is the thickness of the sample. Considering that the overall signal of the ACB is due to the difference from the signals produced at coils localized at $z=0$ and $z=-d$, and because we are concerned with samples very close to the lower set of coils, the field detected by the ACB, after substitution of Eqs. (3), (4), and (5) into Eq. (2), will be given by[7]

$$dB_z=K\cdot I(t)\frac{2(-z')^2-[(-x')^2+(-y')^2]}{[(-x')^2+(-y')^2+(-z')^2]^{5/2}}C(x',y',z')\frac{2(z'+a)^2-(x'^2+y'^2)}{[x'^2+y'^2+(z'+a)^2]^{5/2}}dx'dy', \quad (6)$$

where

$$K=\left(\frac{\mu_0}{4\pi}\right)^2\left(\frac{\mu}{\mu_0}-1\right)\frac{\pi b^2\epsilon}{\rho}N_{\mathrm{EXC}}. \quad (7)$$

To obtain the magnetic field due to an extended source, expression (6) must be integrated over the dimensions x' and y' of the sample yielding a total magnetic field given by

$$B_z^{\mathrm{total}}(x,y,t)=K\cdot I(t)\int_{Y_1}^{Y_2}\int_{X_1}^{X_2}\frac{2(-z')^2-[(x-x')^2+(y-y')^2]}{[(x-x')^2+(y-y')^2+(-z')^2]^{5/2}}C(x',y',z')\frac{2(z'+a)^2-(x'^2+y'^2)}{[x'^2+y'^2+(z'+a)^2]^{5/2}}dx'dy'. \quad (8)$$

Using the conventional notation for summation of continuous functions,[15] the integral above can be discretized as

$$B_z^{\mathrm{total}}[n,m,t]=K\cdot I(t)\sum_{m'=Y_{\mathrm{MIN}}}^{Y_{\mathrm{MAX}}}\sum_{n'=X_{\mathrm{MIN}}}^{X_{\mathrm{MAX}}}\frac{2(-z')^2-[(n-n')^2+(m-m')^2]}{[(n-n')^2+(m-m')^2+(-z')^2]^{5/2}}C[n',m',z']\frac{2(z'+a)^2-(n'^2+m'^2)}{[n'^2+m'^2+(z'+a)^2]^{5/2}}. \quad (9)$$

The signal detected by the ACB at each position is proportional to time varying magnetic flux threading the coils. To calculate the discrete magnetic flux function $\Phi[n,m,t)$ is equivalent to the bidimensional discrete convolution of the magnetic field with the circular symmetric step function[4,15] $S[n,m]$, defined as

$$S[n,m]=\begin{cases}1 & r\leqslant b\\ 0 & c>b\end{cases},\quad \text{where}\quad r=[(n\Delta x)^2+(m\Delta y)^2]^{1/2}\quad \text{thus}$$

$$\Phi[n,m,t)=S[n,m]*B_z^{\mathrm{total}}[n,m,t). \quad (10)$$

Considering that the detector is made sensitive only to the magnetic field with the time dependence of the excitation current $I(t)=I_0\sin(2\pi ft)$, the following expression can be obtained for the voltage detected from an extended sample:

$$V[n,m,t)=N_{\mathrm{DET}}\frac{d}{dt}\Phi[n,m,t)=2\pi fN_{\mathrm{DET}}\cdot S[n,m]*B_z^{\mathrm{total}}[n,m,t), \quad (11)$$

where f is the frequency of the excitation current and N_{DET} is the number of coils in the detector.

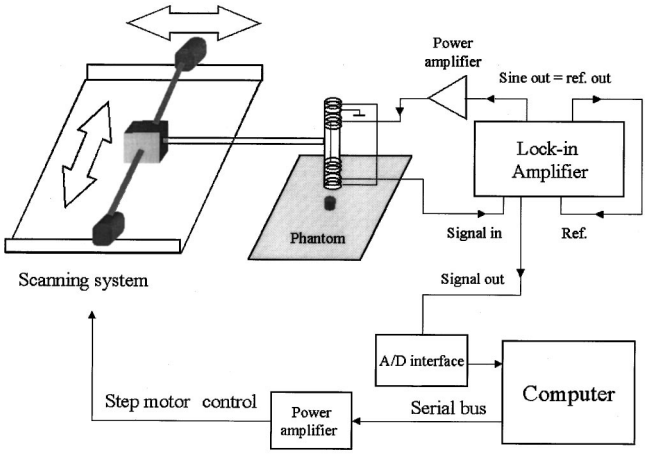

FIG. 4. Experimental setup to scan the samples at different distances. The ACB was attached to a computer controlled x-y scanning stage by a wood arm 1 m long to avoid magnetic interference of this device.

C. The spectral response and the point spread function of the ACB

The convolution of Eq. (11) can be accomplished in the spatial frequency domain using the fact that the Fourier transform of the step function, $s(\omega_x,\omega_y)$, is given by[4,15]

$$s(\omega_x,\omega_y)=\frac{J_1[b\omega]}{b\omega/2}, \tag{12}$$

where J_1 is the Bessel function of the first kind, the spatial frequency $\omega=(\omega_x^2+\omega_y^2)^{1/2}$, $\omega_x=2\pi/k_x$, $\omega_y=2\pi/k_y$ and b is the radius of the detecting coil. Considering that the first set of zeros $J_1(b\omega)$ is localized on a circle with radius[19] $3.83/b$, it can be concluded that the ACB acts like a low pass filter with cutoff frequency $\omega_c=3.83/b$. In accordance with Roth, Sepulveda, and Wikswo[4] this is an important feature because it assures that the major part of the spatial frequencies about the image of a sampled object is localized in a limited bandwidth. According to the sampling theorem the image must be sampled N times in each direction, to avoid aliasing such that the following sampling frequency will be obtained:

$$\omega_s \geqslant 2\omega_c \cong \frac{7.66}{b}\ \text{samples/cm}. \tag{13}$$

This implies that during the processing of the images all signals with frequencies above ω_c will be considered as noise. Thus, the discretized spectrum of the step function will be zero at coordinates given by

$$\sqrt{k_x^2+k_y^2}=\left[\frac{3.83}{b}\cdot\frac{\Delta}{\pi}\cdot N\right]\ \text{cm}^{-1}, \tag{14}$$

where Δ is the frequency of spatial sampling and N is the number of sampled points, k_x and k_y are the wave numbers in both x and y directions.

Using the convolution theorem in Eq. (11) for the voltage in the spatial domain, the voltage can be rewritten in the spatial frequency domain as

$$\nu(k_x,k_y)=2\pi f N_{\text{DET}}\cdot b(k_x,k_y)\cdot s(k_x,k_y). \tag{15}$$

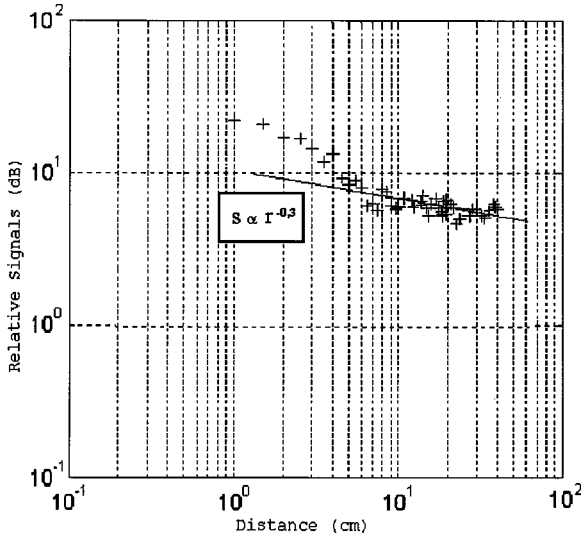

FIG. 5. The dependence of the signal (S) for various distances of the phantom from the sensor shows a more complex dependence with the distance; for distances greater than few centimeters the signal $S\propto r^{-0.3}$.

The voltage detected by the ACB due to an extended source [Eq. (9)] may also be rewritten as

$$V[n,m,t]=[2\pi f N_{\text{DET}}K\cdot I(t)]\cdot S[n,m]*\frac{2(-z')^2-[n^2+m^2]}{[n^2+m^2+(-z')^2]^{5/2}}*C[n,m,z']\times\frac{2(z'+a)^2-(n^2+m^2)}{[n^2+m^2+(z'+a)^2]^{5/2}}. \tag{16}$$

Equation (16) allows us to determine the concentration of the ferromagnetic material $C[n,m]$. To obtain this the response of the ACB will be modeled as the convolution of $C[n,m]$ with the point spread function of the system $h[n,m]$

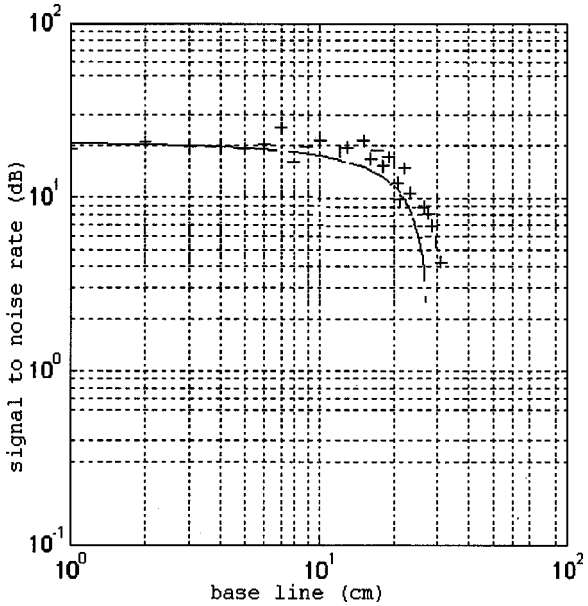

FIG. 6. The dependence of the signal for various base lines of the ac biosusceptometer and a fixed distance of the phantom from the sensor. It can be seen that for distances greater than 6 cm the S/N starts to degrade.

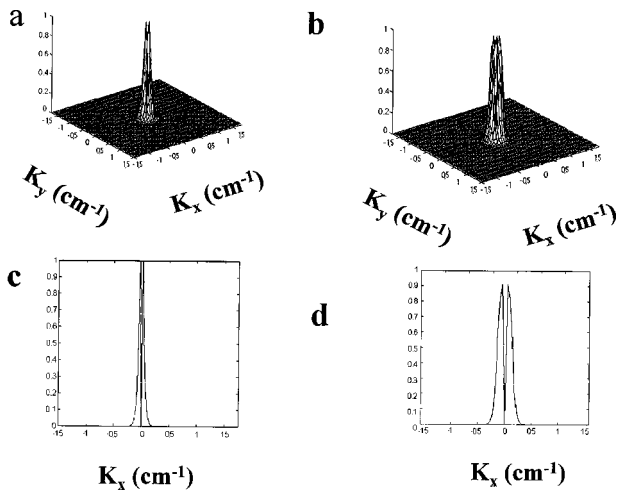

FIG. 7. The simulated (a), (c) and experimental (b), (d) point spread function (PSF) for the ac biosusceptometer. The simulated PSF was obtained through Eq. (20) and the experimental one by scanning a cylindrical phantom of 3 mm diameter and 1 mm thick. It can be seen that the experimental and theoretical PSF shows a pole at origin precluding the use of inverse filtering to restore the images acquired with the ACB.

$$V[n,m]=h[n,m]*C[n,m]. \tag{17}$$

Inserting $=C_0\delta[n,m]$ in Eq. (16), we obtain

$$h[n,m]=[2\pi f I_0 N_{\mathrm{DET}} K\cdot I_0]\cdot S[n,m]*\frac{2(-z')^2-[n^2+m^2]}{[n^2+m^2+(-z')^2]^{5/2}}*\times\delta[n,m]\frac{2C_0}{(z'+a)^3}. \tag{18}$$

Using the Green's function given by Roth, Sepulveda, and Wikswo,[4] discretized in x' and y' directions, defined by

$$G[m,n,z')=\frac{\mu_0 d}{4\pi}z'\frac{1}{[n^2+m^2+z'^2]^{3/2}} \tag{19}$$

expression (18) and Eq. (8) can be rewritten as

$$h[n,m]=\left(\frac{\pi b^2\epsilon I_0}{\gamma}fN_{\mathrm{DET}}N_{\mathrm{EXC}}\right)(\mu-\mu_0)\cdot S[n,m]*\frac{\partial G[n,m,-z')}{\partial z'}*\delta[n,m]\frac{C_0}{(z'+a)^3}. \tag{20}$$

Taking the discrete two dimensional Fourier transform $\Im$ of both sides of Eq. (20), applying the theorem of the discrete convolution and sampling in the frequency space the following expression for the transfer function H is obtained:

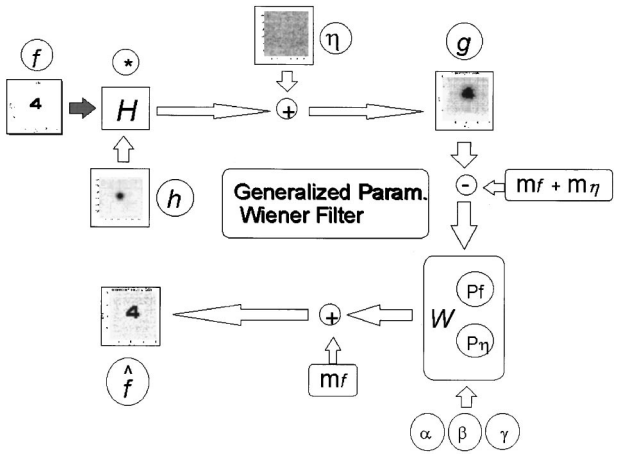

FIG. 8. Schematic diagram showing the simulation procedure to optimize the Wiener filter parameters α, β, γ used to restore the images. An ideal image (f) is convoluted with the experimental PSF and the measured noise spectrum (η) is added, obtaining the simulated image g. The parameters of the filter are adjusted until the best restored image f is obtained. These parameters are then applied to restore all other images.

$$H(k_x,k_y)=\left(\frac{\pi b^2\epsilon I_0}{\gamma}fN_{\mathrm{DET}}N_{\mathrm{EXC}}\right)(\mu-\mu_0)\cdot\Im\{S[n,m]\}\cdot\Im\left\{\frac{\partial G[n,m,-z')}{\partial z'}\right\}\cdot\Im\left\{\delta[n,m]\frac{C_0}{(z'+a)^3}\right\}\Im. \tag{21}$$

Considering the analytical expression for the Fourier transform of the Green function[4]

$$\Im\{G[n,m,-z']\}=\frac{\mu_0 d}{2}e^{\sqrt{\omega_x^2+\omega_y^2}z'} \tag{22}$$

it is possible to obtain the expression for the Fourier transform and its derivative in relation to z':

$$\Im\left\{\frac{\partial G[n,m,-z')}{\partial z'}\right\}=\frac{\mu_0 d}{2}\sqrt{\omega_x^2+\omega_y^2}e^{\sqrt{\omega_x^2+\omega_y^2}z'}. \tag{23}$$

This expression will be zero at $(\omega_x,\omega_y)=(0,0)$. Furthermore[15]

$$\Im\left\{\delta[n,m]\frac{C_0}{(z'+a)^3}\right\}=\frac{C_0}{(z'+a)^3}. \tag{24}$$

From the above equations it can be noted that the discretized spectrum of the system function will be zero at spatial frequencies at $[k_x,k_y]=[0,0]$ and $\sqrt{k_x^2+k_y^2}=[(3.83/b)\cdot(\Delta/\pi)\cdot N]$. This leads to the conclusion that the images acquired must be restored using filtering approaches that avoid the origin of the discrete frequency space, that would produce poles during the inversion process. Therefore inverse filtering techniques should be replaced by Wiener filtering.

III. EXPERIMENTS

In this study phantoms with different shapes containing a gel uniformly labeled with 3% by volume of manganese ferrite ($MnFe_2O_4$) powder were used. The maximum diameter

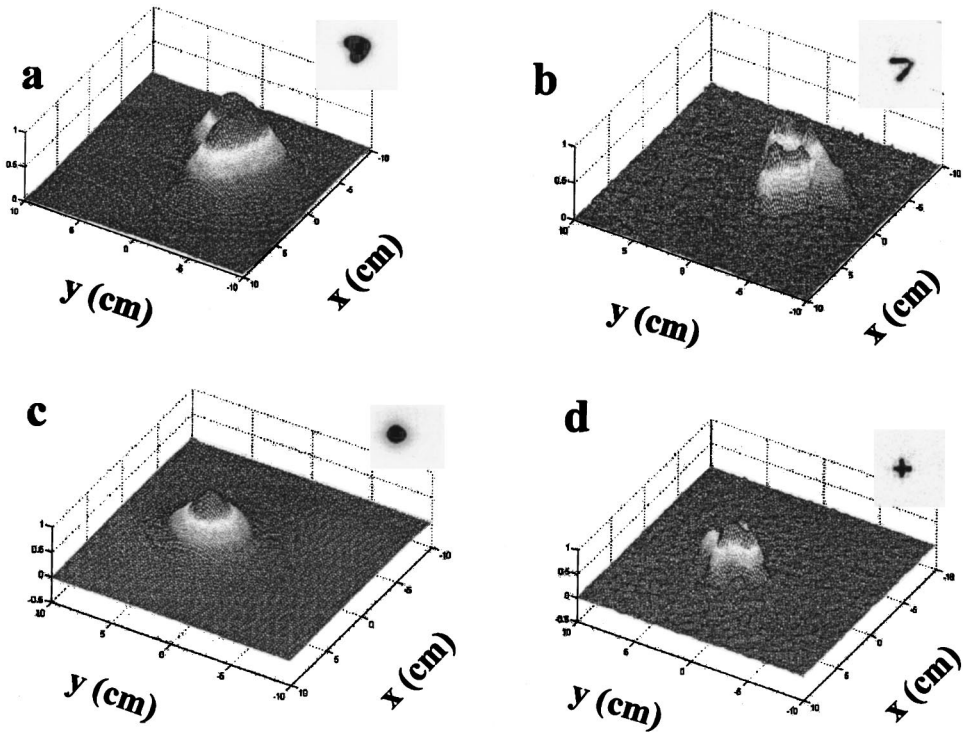

FIG. 9. Typical raw and restored images obtained from two phantoms, a number **7** (a), (b) and a **+** signal (c), (d). The three dimensional plot and plane projection (inset, right upper corner) are shown. It can be seen that the image processing method produces a good improvement in definition and resolution. The variation in intensity is due to nonuniform distribution of the magnetic material inside the phantom.

of ferrite was 125 μm, the density was 4.88 g/cm^3, and magnetic permeability[7] $\mu_r = 3000$. These ferrite particles are used as magnetic tracers in test meals for *in vivo* experiments at the same concentration used in this work. The ac biosusceptometer (ACB) shown in Fig. 2, was excited by a 10 kHz sinusoidal current in the pair of exciting coils producing a magnetic field on the order of 0.1 mT at the measuring site. The difference signal detected by a pair of sensor coils was sent to a digital lock-in amplifer (SR 530 two phase lock-in amplifier, Stanford Research System, California). Base lines (distance between sensor coils) could be varied between 1 and 15 cm. The inductance value of each exciting and sensing coil was 0.56 mH and the resistance 5 Ω. The ACB was attached to a computer controlled *x-y* scanning stage by a rigid arm 1 m long made of wood to avoid magnetic interference. An area of (20×20) cm^2 was scanned in 30 min. Figure 4 shows the experimental setup. When the phantom, for example, a number 7 and **+** signal, both 2 cm wide, is made to enter the magnetic field a difference in voltage is generated across the sensor coils. Acquisition of the biomagnetic signal from the lock-in amplifier was done by means of an analog/digital (A/D) board (TECMAR LabMaster 16) with a 12 bit resolution. Data analysis and visualization were performed on a Pentium PC computer. Signal processing was done using MATLAB® software.

IV. RESULTS AND DISCUSSION

An important parameter in a gradiometric detection system is the base line, the distance between sensor coils. Because this device works as a spatial filter,[20] the base line will control the cutoff spatial frequency of detected signals. Usually the spatial response of a gradiometer can be experimentally evaluated by placing a point source (magnetic dipole) at different distances of the gradiometer and measuring its response.[21] This procedure is highly dependent on the relative dimensions of the source and the detection coil. In our case an alternative procedure was employed. Initially phantoms of different shapes containing the test meal were scanned at different distances from the ACB and the average power spectrum (P_f) was determined for each. At these same distances the power spectrum (P_η) of noise was measured by placing a plane with a very thin homogeneous distribution of ferrite powder. The noise was calculated by averaging the response of five scans. The quantity of ferrite used in these phantoms to assess the noise power spectrum was barely enough to elicit a response of the ACB. This procedure to detect the noise will measure the total noise, including far sources, vibrations, and other interference during the scanning process. Figure 5 shows the dependence of the signal for different distances of the phantom from the sensor. For distances r greater than 5 cm the S/N rate decays slowly as $r^{-0.3}$ allowing that susceptometric images can be obtained with the present device. In another experiment the distance of the scanning plane to the lower detection coil of the gradiometer was constant (2 cm) and the base line was varied. Figure 6 shows the signal/noise for the same phantom as a function of the base line revealing that for a base line greater than 6 cm the S/N plot starts to degrade. A possible explanation for this behavior would be the greater influence of far sources and to a less extent the inherent mechanical instability of gradiometers with longer base lines. The base line chosen for the practical measurements was 5 cm with the ACB sensor 1–2 cm above the phantom. With these distances it was possible to assure a good noise rejection without loss of the signal produced from the phantom. The point spread function (PSF) (also named *impulse response of the system* in current signal processing literature) was obtained experimentally by scanning a 3-mm-diam, 1-mm-thick cylin-

drical ferrite phantom; the image obtained after averaging 20 samplings was used to obtain the experimental PSF. There is a good agreement with the theoretical expression for the PSF obtained in a previous section (Fig. 7), showing a null value at the origin. Figure 8 summarizes the approach to obtain the appropriate parameters for the Wiener filtering. Initially a template image f was generated and a convolution with the experimental PSF h was obtained. The blurred image was added to the experimental noise η to simulate a typical image obtained by the actual scanning process. Because the Wiener filter acts on a signal of zero mean value, the mean values of the noise m_f and the image m_η were subtracted from the blurred image. Knowing the average power spectrum of the image P_f and the noise P_η the parameters of the Wienver filter α, β, and γ (that set the threshold limit for H_γ^{-1}) can be adjusted to produce the best image. Subsequently, the mean value of the image m_f is added back to recover the brightness of the original image f. Various criteria may be used to adjust the parameters of the filter. We optimized the retrieval of the contours of the acquired image. Simulations determined that the best value of the parameter α is 10^5. The quality of the images was not sensitive to the parameter β and it was set equal to 1.

For actual images of different shapes an average S/N of 27 dB was obtained after optimization of the gradiometer. Simulations indicated that the S/N must be at least 40 dB in order to allow a restoration of acceptable quality. Thus some signal conditioning techniques must be applied before the restoration can be used. Figure 9 shows the raw image obtained after scanning a phantom and a typical restored image. It can be seen that the essential features of the phantom are obtained.

In summary, these initial results show that ACB can be successfully used to generate images with moderate spatial resolution. Efforts are under way to build a more sensitive multichannel system that will make acquisition times shorter, compatible with physiological processes that could be examined with this device. After such improvements we intend to use this device to generate images of the gastrointestinal tract.

ACKNOWLEDGMENTS

This work was based on an M.S. dissertation presented at the University of São Paulo in 1995, partially supported by the Brazilian Agencies: PRONEX, CAPES, FAPESP, and CNPq. The technical assistance from E. de Paula, E. Navas, and M. Oliva is also appreciated.

[1] R. A. Erol, P. Cherian, R. H. Smallwood, B. H. Brown, and K. D. Bardhan, Physiol. Meas. **17**, A141 (1996).
[2] M. Ikeya and H. Ishii, J. Magn. Reson. **88**, 130 (1990).
[3] C. M. Smith and A. D. Stevens, Br. J. Radiol. **67**, 1186 (1994).
[4] B. J. Roth, N. G. Sepulveda, and J. P. Wikswo, Jr., J. Appl. Phys. **65**, 361 (1989).
[5] M. Moreira, L. O. Murta, and O. Baffa, Phys. Med. Biol. **39**(a), 633 (1994).
[6] J. R. A. Miranda, O. Baffa, R. B. Oliveira, and N. M. Matsuda, Med. Phys. **19**, 445 (1992).
[7] O. Baffa, R. B. Oliveira, J. R. Miranda, and L. E. A. Troncon, Med. Biol. Eng. Comput. **33**, 353 (1995).
[8] R. B. Oliveira, O. Baffa, L. E. A. Troncon, J. R. A. Miranda, and C. R. Cambrea, Eur. J. Gastroent. Hepatol. **8**, 491 (1996).
[9] J. R. A. Miranda, R. B. Oliveira, P. L. Sousa, F. J. H. Braga, and O. Baffa, Phys. Med. Biol. **42**, 1791 (1997).
[10] N. A. Daghastanli, F. J. H. N. Braga, R. B. Oliveira, and O. Baffa, Physiol. Meas. **19**, 413 (1998).
[11] M. Forsman, L. Hultin, and H. Abrahamsson, in *Biomagnetism: Fundamental Research and Clinical Applications. Studies in Applied Electromagnetics and Mechanics*, edited by C. Baumgartner, L. Deecke, G. Stroink, and S. J. Williamson (Elsevier, Amsterdam, 1995), Vol. 7, p. 739.
[12] M. Basile, M. Neri, A. Carriero, S. Casciardi, S. Comani, C. Del Gratta, L. G. Donato, S. Di Luzio, M. A. Macri, A. Pasquarelli, V. Pizzela, and G. L. Romani, Dig. Dis. Scie. **37**, 1537 (1992).
[13] A. C. Bruno, J. Appl. Phys. **82**, 1 (1997).
[14] P. E. Cruvinel, R. Cesareo, S. Crestana, and S. Mascarenhas, IEEE Trans. Instrum. Meas. **39**, 745 (1990).
[15] J. S. Lim, *Two-Dimensional Signal and Image Processing* (Prentice–Hall, Englewood Cliffs, NJ, 1990).
[16] J. P. Wikswo, Jr., N. G. Sepulveda, and I. M. Thomas, in Ref. 11, p. 789.
[17] S. Tan, Y. P. Ma, I. M. Smith, and J. P. Wikswo, Jr., IEEE Trans. Magn. **32**, 230 (1996).
[18] E. Weber, *Electromagnetic Fields: Theory and Applications*, *Mapping of Magnetic Fields* (Wiley, New York, 1951), Vol. 1.
[19] M. R. Spiegel, *Mathematical Handbook of Formulas and Tables* (McGraw–Hill, New York, 1990).
[20] A. C. Bruno, P. Costa Ribeiro, J. P. von der Wied, and O. Symko, J. Appl. Phys. **59**, 2584 (1986).
[21] J. Vrba, A. A. Fife, M. Burbank, H. Weinberg, and P. A. Bricket, Can. J. Phys. **60**, 1060 (1982).